Supplement of Atmos. Chem. Phys., 19, 1901–1913, 2019
https://doi.org/10.5194/acp-19-1901-2019-supplement

Atmospheric Chemistry and Physics
Open Access
EGU

Supplement of

Relationship between Asian monsoon strength and transport of surface aerosols to the Asian Tropopause Aerosol Layer (ATAL): interannual variability and decadal changes

Cheng Yuan et al.

Correspondence to: Zhanqing Li (zhanqing@umd.edu) and William K. M. Lau (wkmlau@umd.edu)

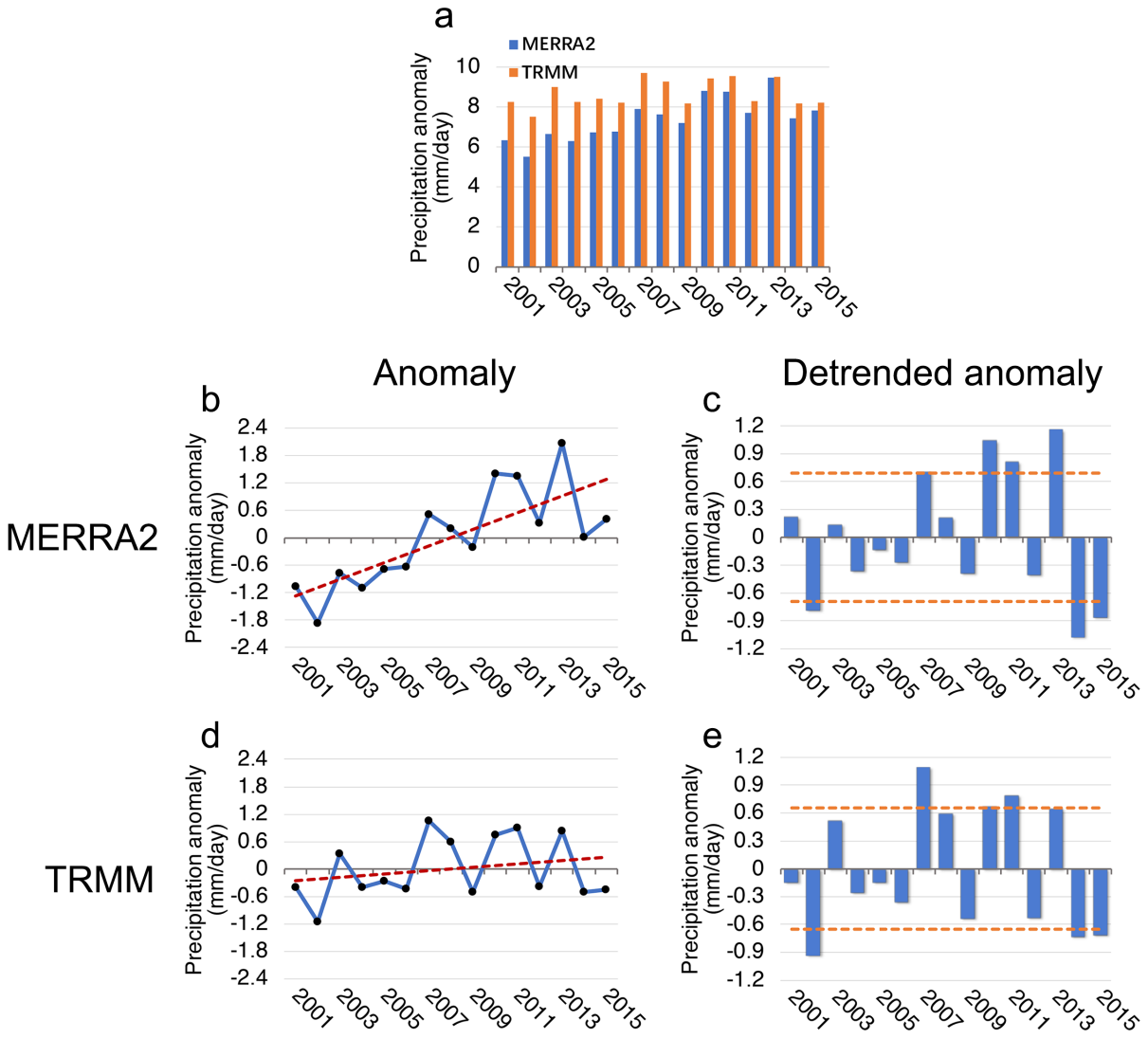

Figure S1. Validation of precipitation by TRMM observatinal data: (a)Comparison of precipitation time series from 2001-2015 over the SASM region (5°N-30°N, 70°N-95°E) from TRMM (orange) and MERRA2 (blue). (b) and (d)Time series of the precipitation anomaly from 2001-2015 (with the trend line in red). (c) and (d)The de-trended distribution (with standard deviations in orange).

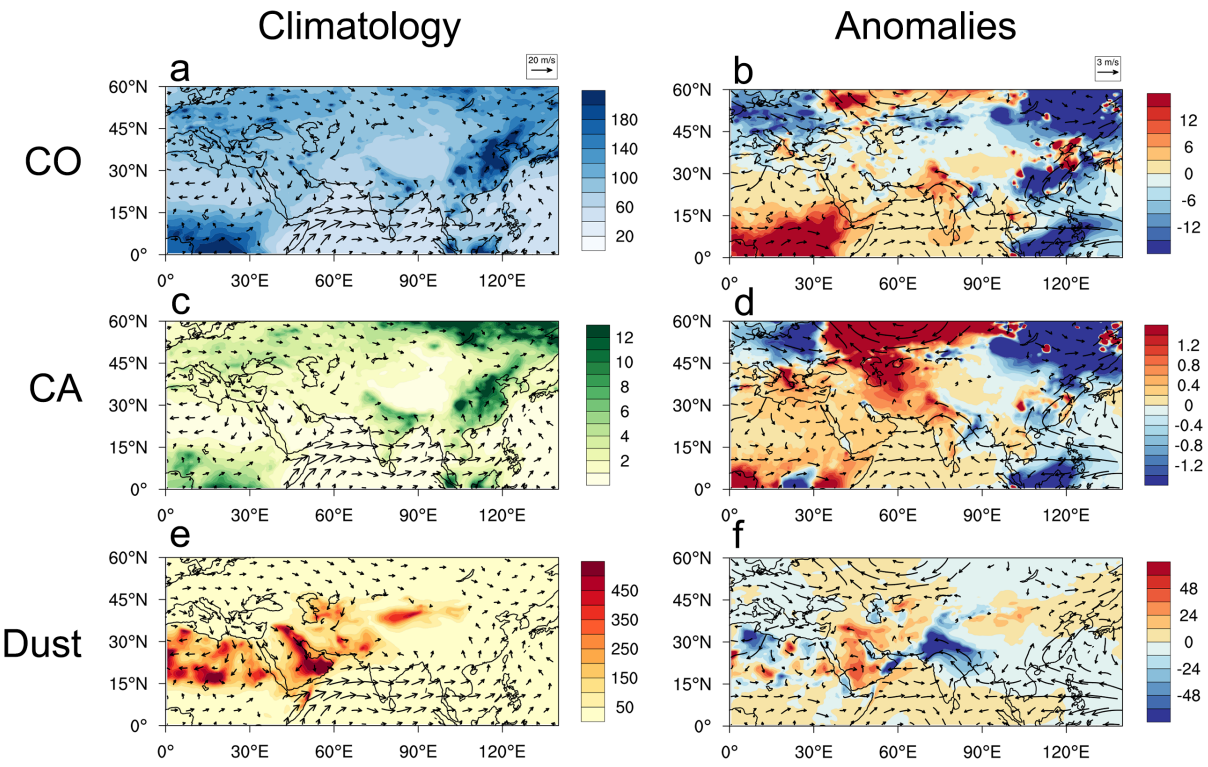

Figure S2. Spatial distributions of climatological (left panels) and anomalous ('strong' minus 'weak', right panels) mass concentrations of CO (ppbv), CA, (ppbm), and dust (ppbm). The climatological 850-hPa wind field and wind field anomalies (arrows, in m s^{-1}) are superimposed on (a, c, e) and (b, d, f), respectively.

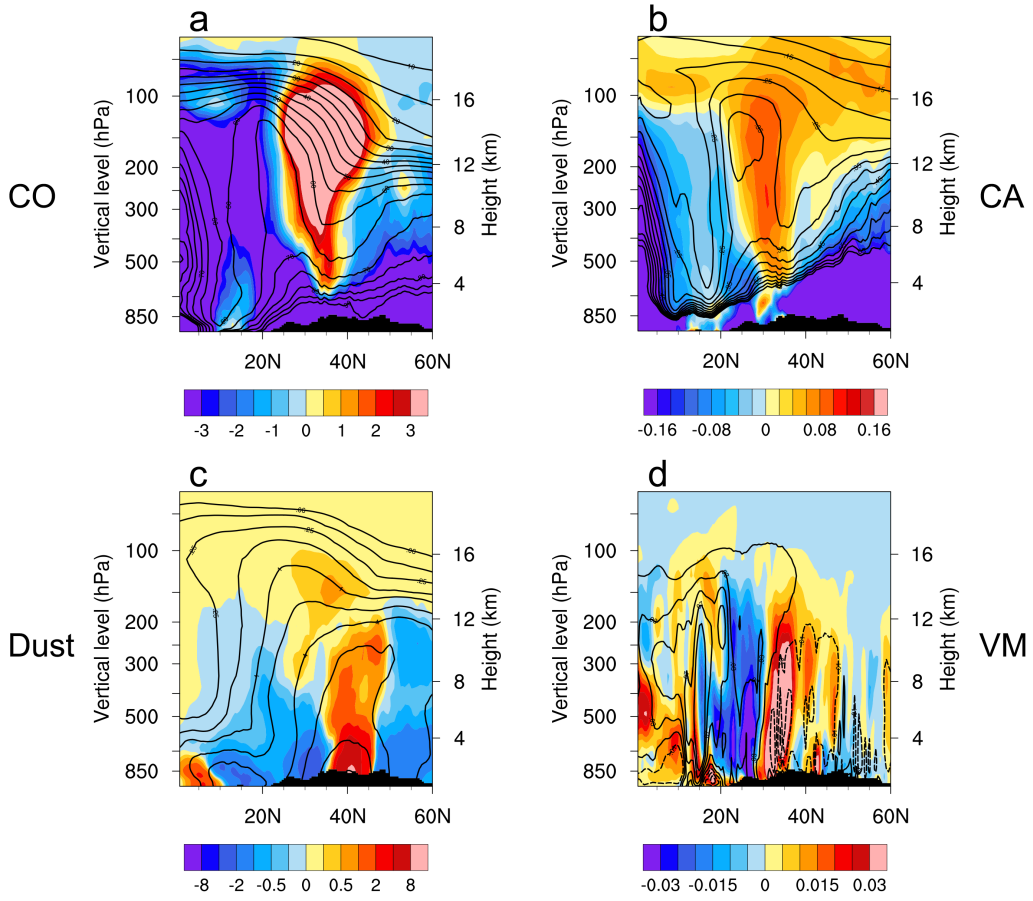

Figure S3. Latitude-height cross-sections (0°N-60°N) of (a) CO (ppbv), (b) CA (ppbm), (c) dust (ppbm), and (d) vertical motion (Pa s^{-1}) anomalies between strong and weak monsoon years ('strong' minus 'weak') averaged over the SB region (100°E-105°E) during July-August, superimposed with the climatological mean of weak monsoon years (black contours). For vertical motions in (d), solid (dashed) contours indicating ascent (descent).

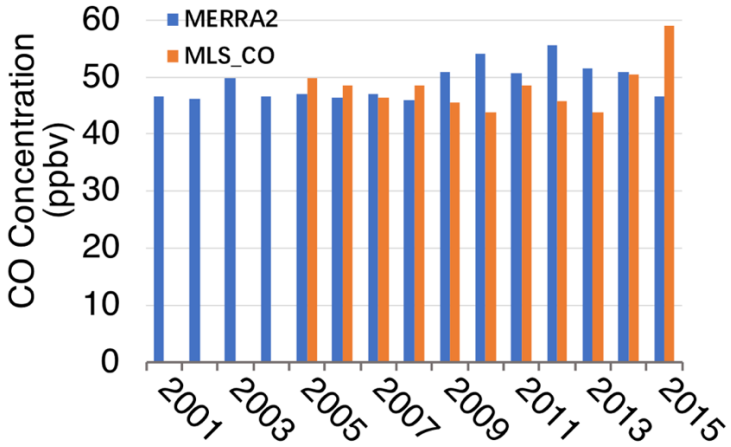

Figure S4. Comparison of the time series of CO concentration at 100 hPa from 2001-2015 over the selected region (25°N-35°N, 60°N-120°E) from MLS_CO (orange) and MERRA2 (blue).

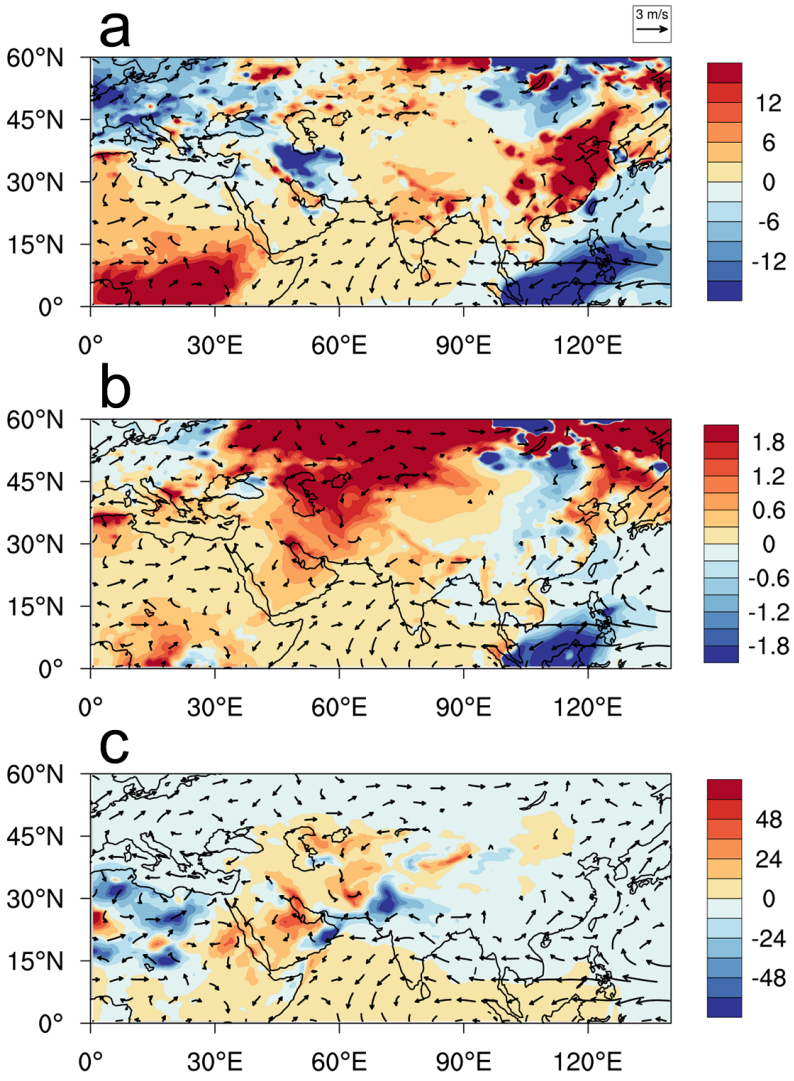

35

Figure S5. Anomalous 850 hPa wind (arrows, in m s^{-1}) and surface loading of (a) CO (ppbv), (b) CA (ppbm), (c) dust (ppbm) between Late Part years and Early Part years ('Late' minus 'Early') during July to August.

40

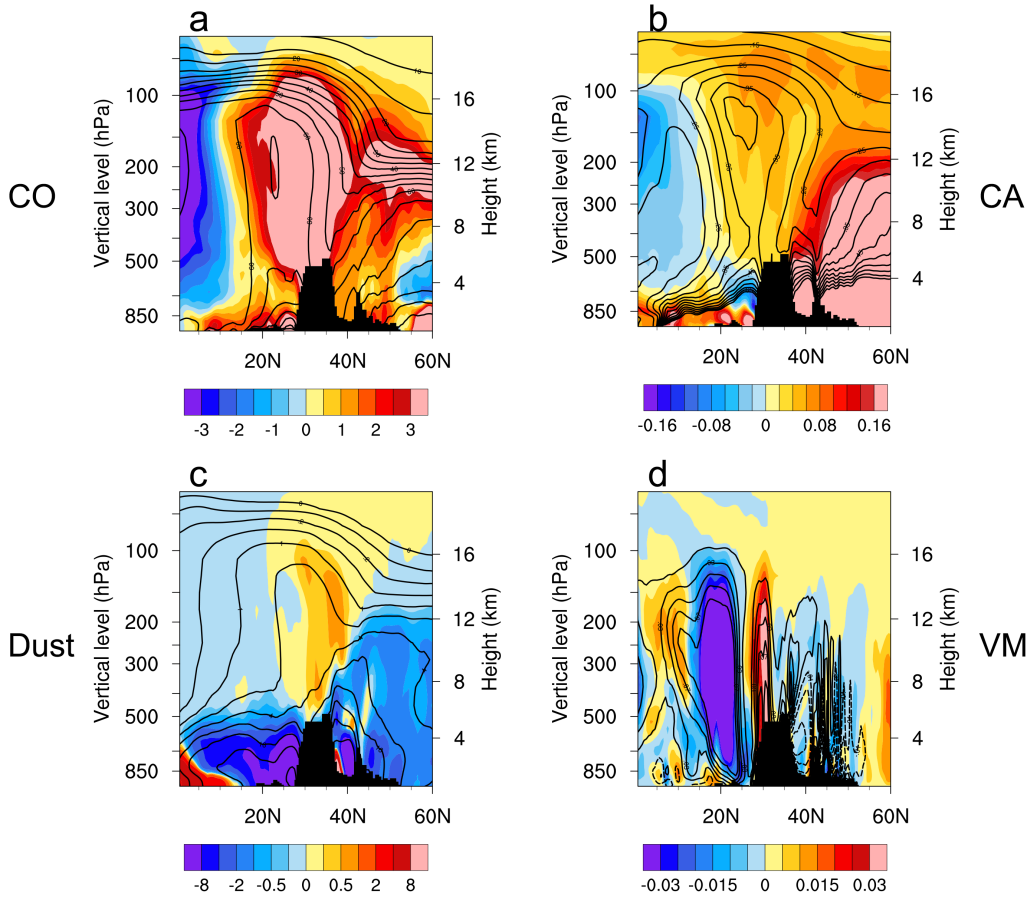

Figure S6. Latitude-height cross-sections (0°N-60°N) of (a) CO (ppbv), (b) CA (ppbm), (c) dust (ppbm), and (d) vertical motion (Pa s^{-1}) anomalies between Late Part years and Early Part years ('Late' minus 'Early') averaged over the HGP region (80°E-85°E) during July-August, superimposed with the climatological mean of Early Part years (black contours). For vertical motions in (d), solid (dashed) contours indicating ascent (descent).

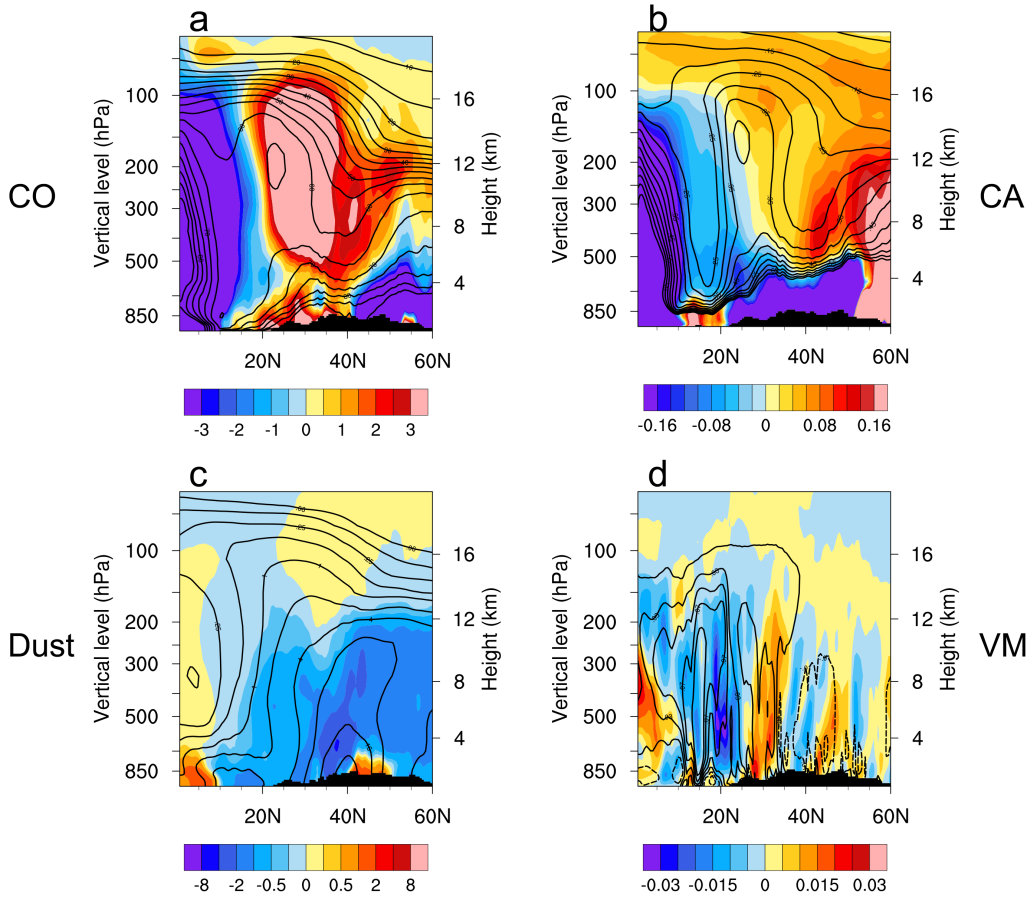

Figure S7. Latitude-height cross-sections (0°N-60°N) of (a) CO (ppbv), (b) CA (ppbm), (c) dust (ppbm), and (d) vertical motion (Pa s^{-1}) anomalies between Late Part years and Early Part years ('Late' minus 'Early') averaged over the SB region (100°E-105°E) during July-August, superimposed with the climatological mean of Early Part years (black contours). For vertical motions in (d), solid (dashed) contours indicating ascent (descent).